Brimacombe Memorial Symposium, Vancouver, Canada, October 1-4, 2000, Met Soc., CIM, pp. 595-611.

Analysis of the Potential Productivity of Continuous Cast Molds

C. Li and B.G. Thomas
University of Illinois
Dept. of Mechanical and Industrial Engineering
1206 West Green Street
Urbana, Illinois, USA 61801
bgthomas@uiuc.edu

ABSTRACT

Heat transfer in the mold is the heart of the continuous casting process and its quantitative analysis was pioneered by Keith Brimacombe. With many different processes currently competing, it is appropriate to apply modeling to investigate the theoretical limits of continuous casting speed and productivity. The heat transfer rate during solidification processes drops with time so the shell thickness at mold exit drops with increasing casting speed. A computational heat flow model similar to those of Brimacombe is applied to investigate the consequences of very high casting speed on shell thickness at mold exit. Next, a finite-element stress model is applied to predict the minimum shell thickness at mold exit that should have sufficient strength to avoid rupture due to longitudinal tearing of the weak shell under the forces of ferrostatic pressure. The critical shell thickness is predicted to be on the order of 3 mm for most grades and casting conditions. The models are then applied to predict maximum casting speeds for different steel grades, section sizes, and mold lengths. The theoretical limits to casting speed are predicted to be extremely high, exceeding 21 m/min for a conventional 800-mm long, 200-mm square bloom mold, which corresponds to 3.5 million tonnes per year. The infeasibility of these high limits in practice is due to other problems, such as achieving shell thickness uniformity and liquid flux lubrication. This work suggests that if shortening mold length can solve lubrication, taper, and other problems, then it should be explored as a potential means to increase productivity.

INTRODUCTION

As the steel industry continues to improve quality and reduce cost, there is growing interest in maximizing the productivity from a single continuous casting machine. Many different processes are currently competing, from conventional thick slab and blooms to thin slabs and strip casting, whose economic feasibility depends on their eventual productivities. Considering the high cost of plant experiments, it is appropriate to apply computational modeling to explore the theoretical limits of continuous casting speed and productivity.

Many researchers have investigated heat transfer and shell solidification in the mold during the continuous casting of steel [1-6]. However, Keith Brimacombe and coworkers were the first to apply advanced computational models of both heat flow [1, 7] and stress [8, 9] to gain quantitative insight into these phenomena, which comprise the heart of the process [6]. Thus, it is fitting to apply such models to explore the limits of the process at this symposium to honor his memory.

Productivity increases with increasing casting speed and increasing cross-section area. The casting speed is limited by several different phenomena, listed below.

1) Excessive level fluctuations and waves at the meniscus become worse with greater casting speed. This can cause surface quality problems and even sticker breakouts. This problem can be addressed by changing nozzle design (directing the flow more downward, possibly by adding a bottom vertical port), applying electromagnetic forces, changing mold fluxes, and using other methods to control the flow pattern in the mold.

2) Excessive axial strains caused by the oscillation and withdrawal forces needed to overcome friction between the solidifying shell and the interfacial layers in the mold can lead to transverse cracks and breakouts at mold exit. Schwerdtfeger [3] has calculated that these stresses are negligible if the liquid layer of the mold flux can be kept continuous over the entire mold surface.

3) Excessive transverse strains may be generated in the thin shell by the ferrostatic pressure of the liquid pool below the mold. This can lead to longitudinal cracks and breakouts if the shell is not thick enough at mold exit.

4) Any local nonuniformity in the shell growth can lead to locally hot and thin regions in the shell, which can initiate longitudinal cracks and breakouts even if the shell is above the critical thickness on average. This problem, which has been investigated by Brimacombe and others, [10] can be addressed by optimizing mold flux behavior during initial solidification, oscillation practice, and taper design, such that flux lubrication is continuous, the initial heat flux is low and uniform, and the mold wall taper matches the shell shrinkage profile [11]. Peritectic steel grades and austenitic stainless steel are most susceptible to this problem. Superheat delivered from the flowing steel jets can also contribute to

this problem, especially near the narrow faces in slab casting with bifurcated nozzles.

5) Excessive bulging of the strand below the mold can lead to a variety of internal cracks and even breakouts if the bulging is extreme. Bulging can be controlled by choosing short enough support roll spacing, maintaining roll alignment, controlling spray cooling below the mold, and by avoiding sudden changes in roll pitch, sprays, or casting speed.

6) The distance below the meniscus of the point of final solidification of the center of the strand increases in direct proportion with casting speed for a given section thickness, which usually limits the maximum casting speed in a given steel plant. The torch cut-off, spray cooling system, and roll support system all must extend to accommodate this increase in metallurgical length. Contrary to intuition, this metallurgical length cannot be significantly shortened by increasing the spray cooling intensity [12]. This understanding is incorporated in the pioneering work of Brimacombe and coworkers to provide design criteria for spray zones [12, 13].

7) Finally, there are many other special quality concerns which sometimes impose limits on casting speed. For example, in ultra-low carbon steels, a relatively slow upper limit in casting speed is required in order to reduce pencil pipe and other blister defects due to argon bubble entrapment on the inner radius of curved mold casters [14, 15]. Casting speed can only be increased in these situations by careful changes in operating conditions that avoid the specific defects of concern.

Clearly, to increase the casting speed of a continuous casting process requires careful consideration of many different phenomena. The above list shows that at least seven separate criteria must be satisfied, any of which could limit the casting speed for a given operation. In practice, the complex problems associated with transient nonuniformities in the shell growth (criterion 4) are often responsible for limiting casting speed and corresponding production rates. This issue is being addressed elsewhere.

Considering all of the above criteria, the most fundamental limit is criterion 3, which has also received very little attention in previous work. The shell at mold exit must have at least the critical thickness necessary to contain the liquid pool and avoid longitudinal rupture due to excessive creep strain of the thin shell. Thus, this work investigates the theoretical upper limits on casting speed and productivity imposed by this need.

MODEL DESCRIPTION

To explore the critical shell thickness and maximum potential casting speeds, this work applies two-dimensional transient finite element models of heat transfer and stress generation in a thin section through the solidifying shell. The model tracks the evolution of temperature, solidification, stress, and strain in a slice through the solidifying shell as it moves down through the caster [16]. The model domain, illustrated in Figure 1, is a

slice through the solidifying shell at the center of one side of the continuous cast strand. This slice domain is 0.2 mm thick and has a maximum length of half of the strand section size. A fine mesh of 10 nodes per mm was required to achieve acceptable accuracy. This mesh was connected into 3-node and 6-node triangle elements for heat transfer and stress analysis, respectively.

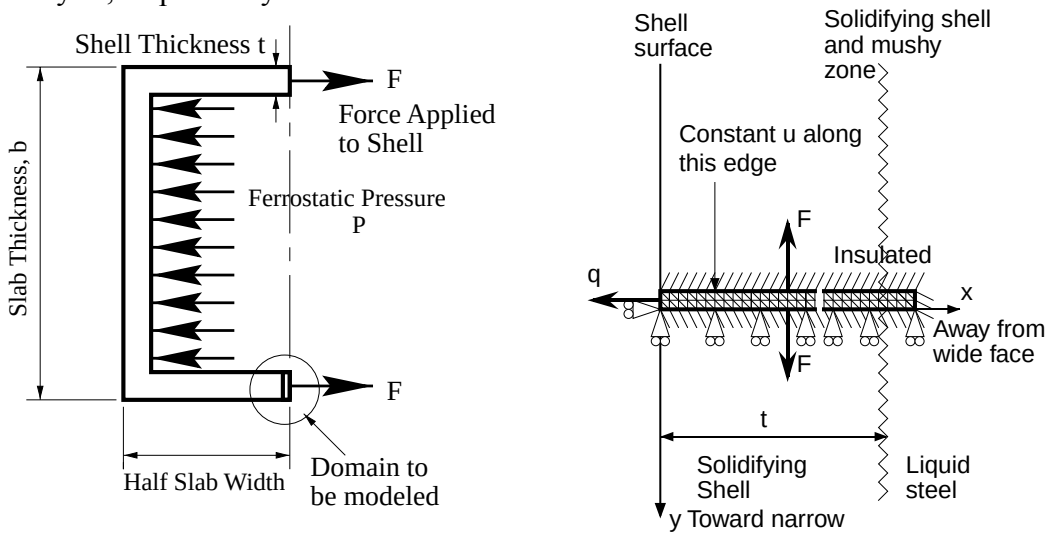

(a) region of shell modeled b) slice model domain with finite element mesh

Figure 1 – Modeling domain

The effects of ferrostatic pressure are modeled by applying a force onto the edges of the solidifying shell domain. This force, F, was evaluated with Equation (1), which balances the stress across the shell at every distance, z, below mold exit with the local ferrostatic pressure, P (Pa), which is simply ρgz.

$$F(N/m) = P(b - 2t)/2 \qquad (1)$$

Heat Flow Model

A mathematical heat flow model similar to those developed by Brimacombe is applied to investigate the consequences of very high casting speed on the thickness and temperature distribution of the shell from the meniscus to mold exit and beyond. Specifically, the heat flow model solves the 2-D transient energy equation, using a fixed Lagrangian grid of 3-node triangular finite elements. Interfacial heat flux is imposed on the thin edge of the domain in Figure 1 as a function of time.

The average heat transfer rate to the continuous casting mold has been measured to drop with time, as illustrated in Figure 2 [1, 2, 4, 5]. This data was compiled from measurements of many processes including thin strip casting, thin slab casting, and conventional billet and slab casting, much of it by Brimacombe [1]. Note that most of the data falls on roughly the same curve, despite the differences between the processes.

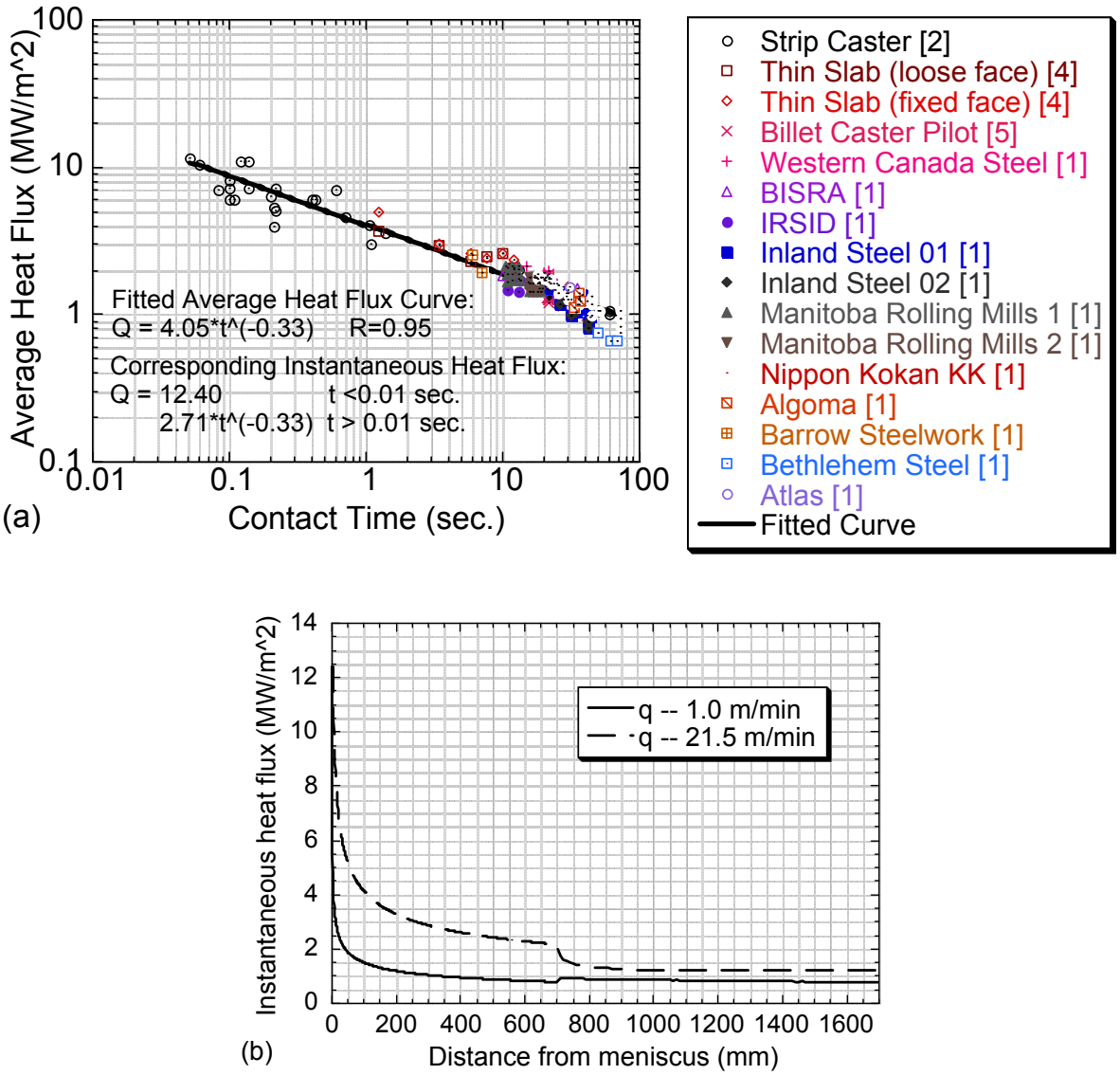

Figure 2 – Heat flux rate

a) Total average heat flux with respect to contact time
b) Instantaneous heat flux with respect to distance below meniscus

Figure 2(a) shows that the average total heat removed while the shell is in the mold depends only on time. Based on these measurements, the following empirical formula is used to describe the average heat flux, $\bar{q}$, as a function of contact time, t_e.

$$\bar{q}(MW/m^2) = 4.05 t_e(\text{sec.})^{-0.33} \qquad (2)$$

This average heat flux curve was then generalized for any continuous casting process. The instantaneous heat flux, q, was obtained by multiplying Equation (2) by t_e and then differentiating. The function was truncated at short times to give:

$$q(MW/m^2) = \begin{cases} 12.40 & t \le 0.01\text{sec.} \\ 2.71t(\text{sec.})^{-0.33} & t > 0.01\text{sec.} \end{cases} \quad (3)$$

By relating the time below the meniscus, t, to the casting speed, this instantaneous heat flux was transformed into a function of distance below the meniscus. Examples are shown in Figure 2(b) for two typical casting speeds.

Stress Model

Starting with stress-free liquid at the meniscus, the stress model calculates the evolution of stresses, strains, and displacements, by interpolating the thermal loads onto a fixed-grid mesh of 6-node triangles. This thermal stress model, CON2D, features an elastic-viscoplastic constutive equation, and is a finite-element FORTRAN program, developed at the University of Illinois [16]. In this program, increments of total strain are divided into elastic strain, thermal strain, inelastic strain, and a pseudo-strain rate accounting for flow of the liquid [17].

Friction between the mold and shell is neglected. This assumes that the liquid flux film is continuous. The out-of-plane z-stress and y-stress are both characterized by the state of generalized plane strain. This allows the simulation of a simple slice to reasonably estimate the complete 3-D stress state, for a long, wide, thin shell. This is the best assumption in the absence of bending or friction. Each slice is constrained by the rest of the shell to remain straight (flat) as it moves down the mold.

Material property data

Four steel grades were considered in this work: 0.003%C, 0.044%C, 0.1%C and 0.44%C carbon steels, which also contain 1.52%Mn, 0.34%Si, 0.015%S and 0.012%P. The solidus and liquidus temperatures, given in Table 1, are based on the non-equilibrium calculations of Won et. al [18]. The temperature-dependent elastic modulus used in this work is discussed elsewhere [23]. A critical strain criterion is used to define failure in a similar manner to that used by Brimacombe [9]. The criterion in this work is based on experiments on carbon steels tabulated and fitted by Won et. al. [19].

Table 1. Solidus and Liquidus Temperatures and Critical Strain

Steel Type	Liquidus (^{o}C)	Solidus (^{o}C)	Critical Strain to Fracture (%)
0.003%C	1524.7	1496.9	6.1
0.044%C	1521.0	1481.7	4.5
0.1%C	1516.0	1460.8	3.4
0.44%C	1485.4	1369.0	1.8

The thermal expansion coefficient is very important for the thermal stress analysis since it directly determines the thermal strain. The TLE functions used in this work [17] are based on solid phase density data by Jablonka [20] and liquid density data from Jimbo and Cramb [21]. They are shown in Figure 3, starting from zero at the solidus reference temperature.

The elastic-viscoplastic constitutive equations are based on model III of Kozlowski [23] for the austenite phase and a power law model in the delta-ferrite phase [16]. Figure 4 shows the stress predicted by these equations as a function of temperature compared with measurements by Wray [22]. It can be seen that δ-ferrite is weaker than austenite. Thus, δ-ferrite will creep faster than austenite under the same stress and is able to support less load for a given strain.

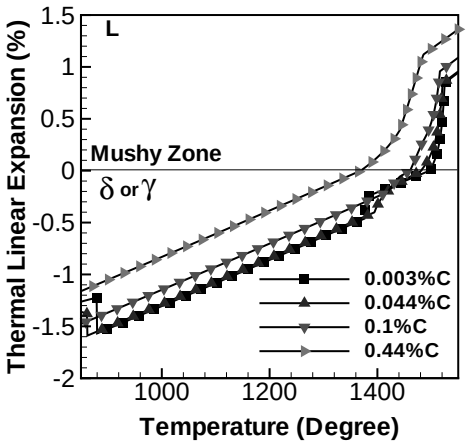

Figure 3 – Thermal linear expansion of steel for different %C (data from [20]and [21])

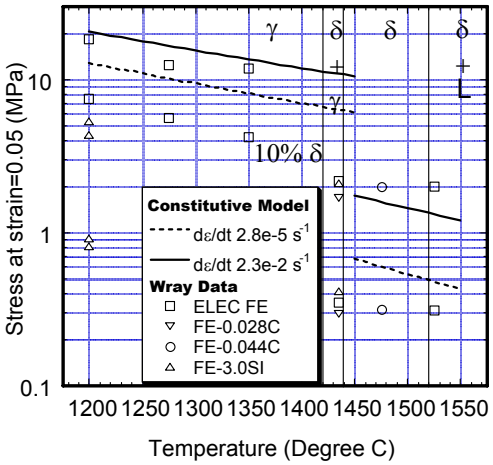

Figure 4 – Comparison of predicted and measured stress, [22] showing δ-ferrite is weaker than γ

MODEL VALIDATION

To validate the thermal stress model, CON2D was used to model a 1-D thermal stress problem of a solidifying metal slab with an analytical solution [24]. Figure 5 compares the temperature and stress distributions through the solidifying slab at various times. The model predictions and the analytical solution are virtually identical.

Next, the results from several CON2D model simulations were compared with shell thicknesses measured for several different high-speed continuous casting processes [2]. The simulations were performed using Eq. 3, which is based on the heat flux measurements in Figure 2a). Shell thickness was defined by a solid fraction of only 0.2, which assumes that most of the liquid is trapped between the dendrites when a shell is drained. The predictions and measurements consistently show how the shell thickness decreases with increasing casting speed. This is because the slight increase in heat flow

rate at smaller times is not enough to make up for the linear drop in total heat flow with decreasing time.

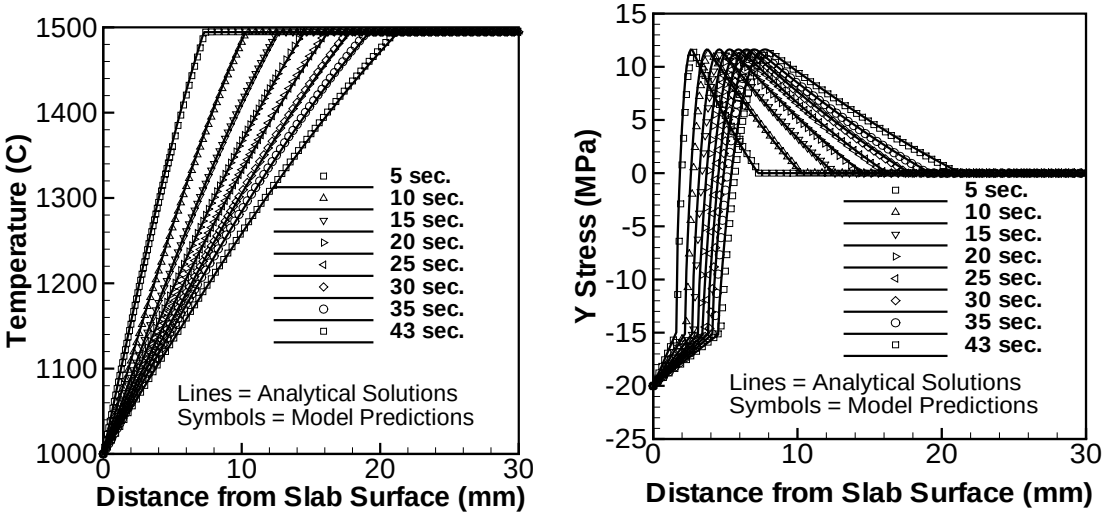

(a) Temperature (b) Stress

Figure 5 – Comparison of Boley and Weiner analytical solutions and CON2D predictions

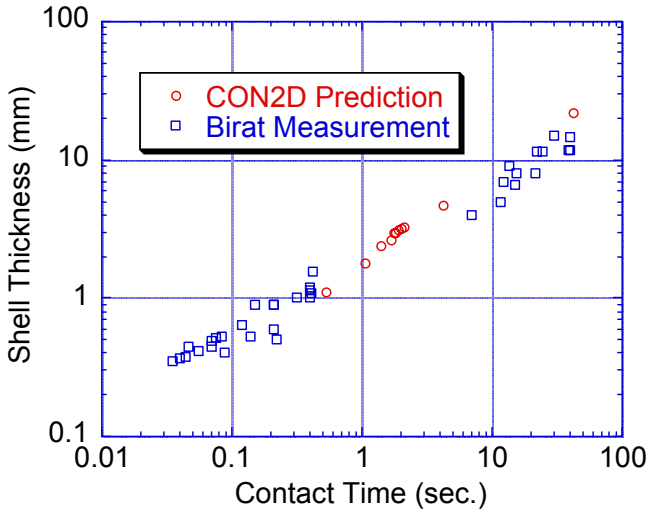

Figure 6 – Comparison of measured and predicted shell thickness

TYPICAL RESULTS

Parametric studies were conducted with the CON2D model to investigate temperature, stress, and critical shell growth for casting speeds ranging from 1.0 to 120 m/min, section sizes from 50 to 400 mm, working mold lengths from 300 to 1200 mm and four different steel grades. Results for two typical simulations are shown in Figures 7 and 8 for 0.044%C steel cast in a 200-mm square bloom mold with 700-mm working mold length (800-mm total length) with casting speeds of 1.0 and 21.5 m/min. The 1.0 m/min case is a normal casting speed used in practice, while the 21.5 m/min case is the critical casting speed for this steel and mold. Figure 7 shows the surface temperature, shell thickness, plastic strain rate and total strain histories. Figure 8 shows the temperature and stress distribution through the solidifying shell just below mold exit for these two cases.

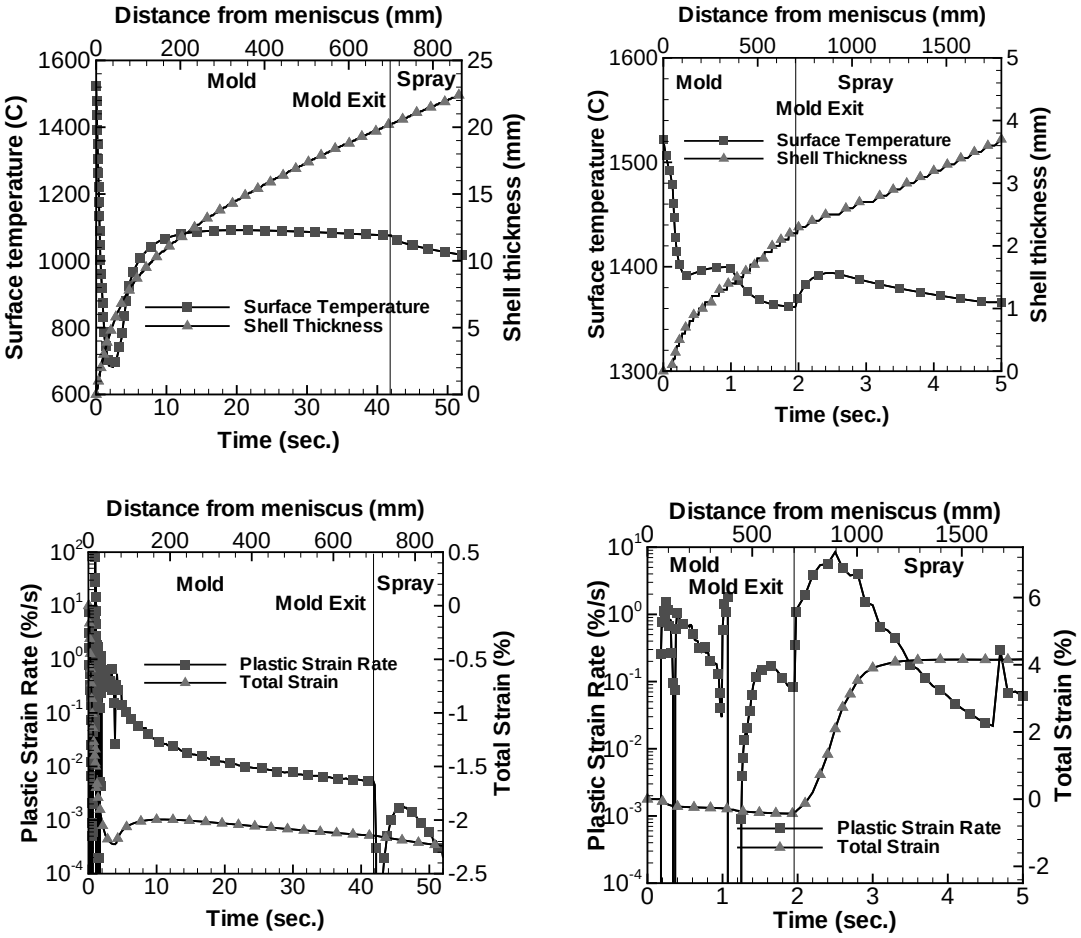

(a) Casting speed – 1.0 m/min (b) Casting speed – 21.5 m/min

Figure 7 – Typical thermal-mechanical histories at strand surface (0.044%C carbon steel cast in 200-mm square 800- mm long mold)

The surface temperature drops sharply just below the meniscus and then reheats. This is due to the very high heat flux expected at the beginning of solidification, regardless of casting speed. Increasing the casting speed reduces the total heat removed

by the mold so generates a hotter and thinner shell at mold exit. As the strand moves below the mold, ferrostatic pressure starts to exert a load on the inside of the shell. At low casting speed, the shell is thick enough to withstand this pressure so the plastic strain rate due to creep is very small (less than 0.01%/s). Thus, the total strain is dominated by the thermal shrinkage of the strand so decreases with distance below the mold.

At high casting speed, however, the thin and hot shell creeps rapidly under the ferrostatic pressure. This generates high plastic strain rates, which reach a maximum of almost 10%/s just below mold exit. This maximum corresponds to the maximum surface temperature, which experiences reheating due to the drop in heat removal in the spray zones relative to the high mold heat removals expected at this casting speed (Figure 2b). The result is a rapid increase in tensile strain below mold exit, which reaches over 4% for this case. If the total strain reaches the critical fracture strain, (Table 1), the shell is assumed to have failed. The creep strain rate continuously drops with distance below mold exit because the increase in shell thickness is much more important than the increase in ferrostatic pressure. Thus, the total strain saturates after about 4 s for this case. In general, the most likely time for failure is in the first few seconds below mold exit, which corresponds to the time when many breakouts experience in practice.

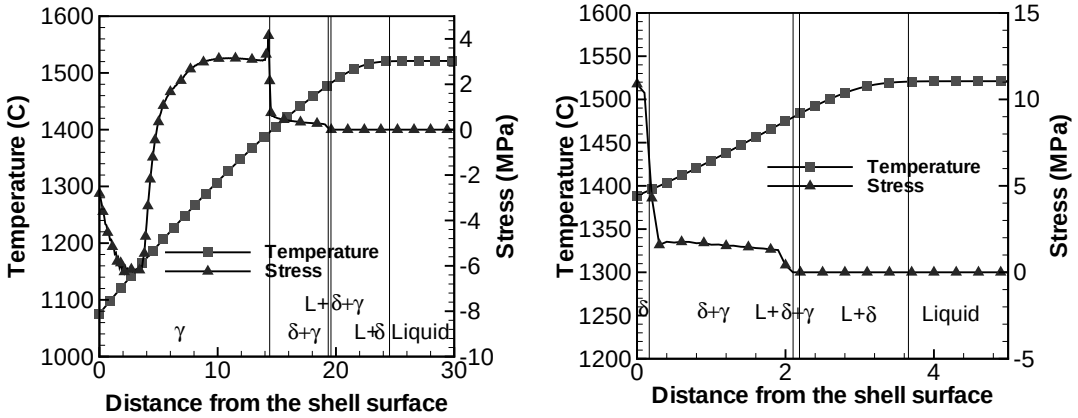

(a) Casting speed: 1.0 m/min (b) Casting speed: 21.5 m/min

Figure 8 – Temperature and stress distribution through the solidifying shell

Figures 8(a) and (b) show the temperature and stress profiles through the thickness of the solidifying shell for the two casting speeds, respectively. Temperature increases almost linearly from the surface temperature (left) to the liquid (right). Naturally, there is no stress in the liquid and there should be virtually no stress in the mushy zone. It is significant to note that there is very little stress generated in the delta-ferrite portion of the solid shell. As the temperature lowers, stress builds up in the cooler parts of the shell and reach a maximum at the shell surface. The colder austenite portion of the shell thus carries most of the stress.

CRITICAL SHELL THICKNESS

The results in the previous section showed that plastic strain due to creep will increase greatly just below the mold exit, if the shell is too hot and thin. The rate of creep strain accumulation decreases as the shell thickens. For each simulation in this study, this accumulation of strain was continued until the plastic strain rate dropped off to below 0.1%/sec. If the total strain at that moment reached the failure strain criterion measured for that steel (Table 1), then the shell was assumed to fail, as a longitudinal crack or breakout. The shell thickness at that time defines a critical shell thickness because the conditions which produce thicker shells never fail. In this work, the critical shell thickness was found for different steel grades, superheats, section sizes and mold lengths by increasing the casting speed until the failure criterion was reached. The effects of each of these variables are shown in Figures 9-12.

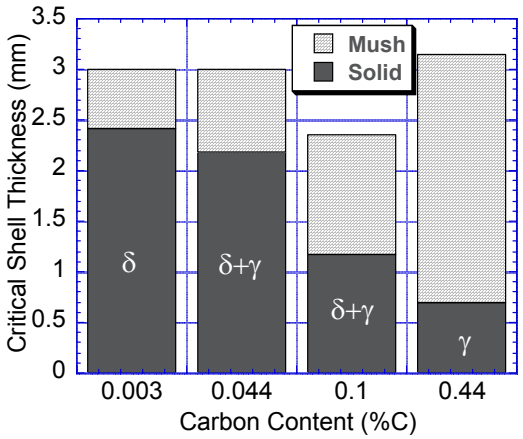

Figure 9 – Carbon content effect on critical shell thickness (200 mm square bloom, 800 mm mold)

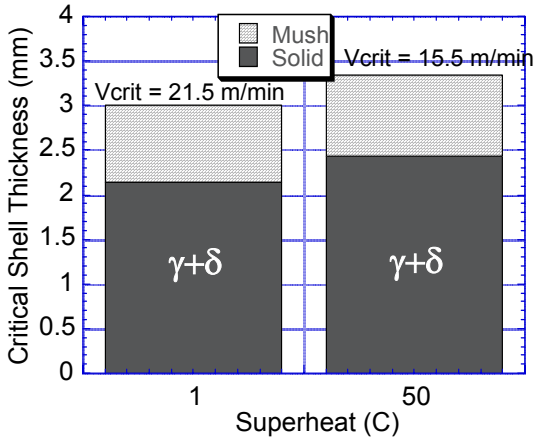

Figure 10 – Super heat effect on critical shell thickness (0.044%C steel cast in 200 mm square bloom, 800 mm long mold)

Figure 9 shows the critical shell thickness for steels with different carbon contents cast under similar conditions. It is interesting that the critical is nearly 3mm for all 4 grades, with the peritectic 0.1%C steel being slightly less. This indicates that the peritectic steel is actually slightly stronger and more crack resistant than the other steels. The fact that this steel is more crack prone in practice is thus due solely to its greater tendency to have shell thickness nonuniformities. This steel grade thereby has a greater chance of having a local thin spot less than the critical thickness.

Figure 9 also shows that the makeup of the shell changes greatly with steel grade. As the carbon content increases, the solid portion of the shell decreases. The shell also becomes stronger, however, because the austenite fraction increases. A much thicker delta-ferrite shell is needed to support the same load. On the other hand, the mushy zone becomes thicker as the carbon content increases with the wider freezing

range. The net result is a critical shell that has about the same thickness, and requires about the same amount of heat removal to produce, for all of the grades.

Increasing superheat leads to a hotter and thinner solidifying shell, for a given heat removal. Consequently, the casting speed needed to produce the critical shell thickness decreases. The critical shell thickness increases only slightly, however, owing to the hotter surface temperature. This slight effect of superheat is shown in Figure 10.

Increasing the section size causes the critical shell thickness increase, as shown in Fig. 11. This is because a thicker shell is needed to withstand the larger ferrostatic load.

Shortening the mold length causes the critical shell thickness to increase, as shown in Figure 12. This is because the contact time is shorter, so the shell is hotter and weaker for a given thickness. Thus, a thicker shell is needed to get sufficient strength.

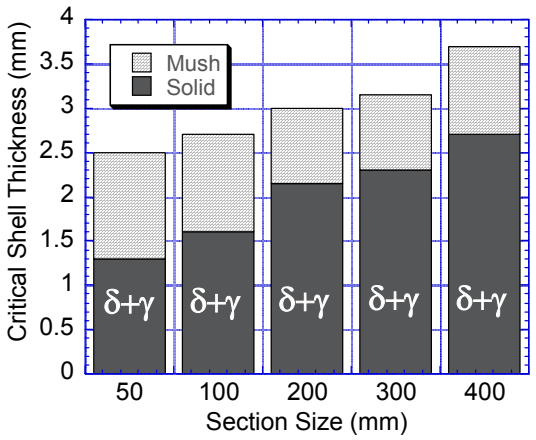

Figure 11 – Section size effect on critical shell thickness (0.044%C steel cast in 800 long mm mold)

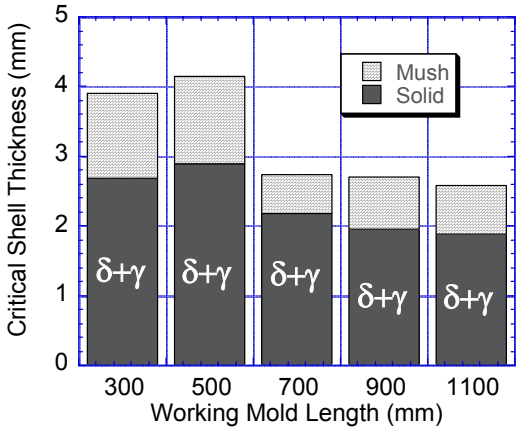

Figure 12 – Working mold length effect on critical shell thickness (0.044%C steel cast in 200-mm bloom)

CRITICAL CASTING SPEED

Increasing the casting speed results in hotter, thinner shells, which experience increased creep strain. This is seen in Figure 13, which shows the total strain (when plastic strain rate drops to 0.1%/s) as a function of casting speed for the 0.044%C steel. The strain which exceeds the fracture criterion (4.5% for this steel) defines both the critical casting speed and the corresponding critical shell thickness, which was discussed in the previous section. The effect of steel grade, section size, and working mold length on critical casting speed are shown in Figure 14.

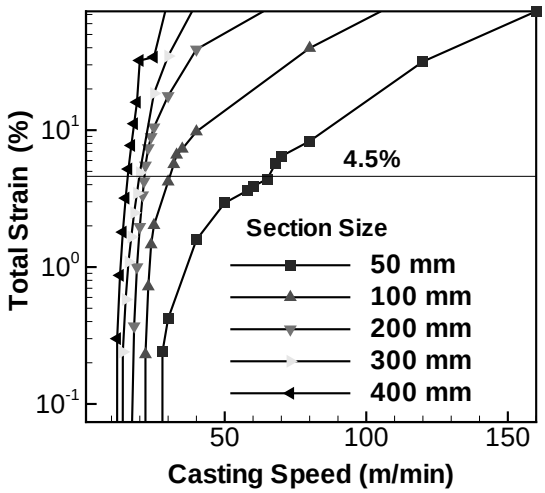

Figure 13 – Effect of casting speed and section size on total strain (0.044%C steel at $\dot{\varepsilon} = 10^{-3}\ s^{-1}$)

The effect of steel grade on critical casting speed is shown in Figure 14(a). The trends correspond naturally with the effect of grade on critical shell thickness. The thinnest critical shell, for 0.1%C steel, can tolerate a highest critical casting speed. Figures 10 and 14(a) both show that increasing the carbon content makes the solid portion of the shell stronger.

Figure 14(b) shows that increasing the working mold length allows higher casting speeds to be tolerated. This is because the contact time increases and leads to a thicker shell at the mold exit. However, increasing the mold length requires increased attention to mold taper lubrication.

In order to maintain good contact between the shell and the mold, and thereby maintain good heat transfer, the mold must be tapered to match the shrinkage of the steel. This task becomes more difficult with a longer mold, which requires a nonlinear taper. In addition, the longer mold allows more time for the temperatures to drop and the liquid flux in the gap to solidify. Friction against the solid flux generates much higher longitudinal stresses in the shell, which could restrict the critical casting speed.

Figure 14(c), shows that increasing the section size should decrease the critical casting speed. This is due to the greater ferrostatic pressure, as discussed for Figure 11. However, the speed drop is less than linear.

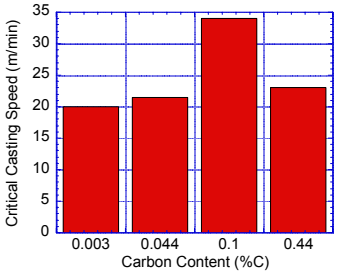

(a) Carbon content (200 mm square bloom, 800 mm mold)

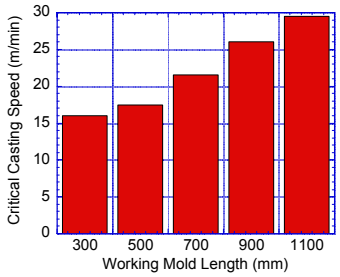

(b) Working mold length (0.044%C steel cast in 200 mm square bloom)

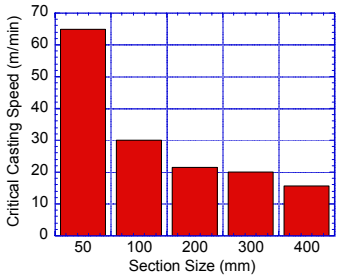

(b) Section size (0.044%C steel cast in 800 mm mold)

Figure 14 –Critical Casting Speed – Influencing Factors

MAXIMIZING PRODUCTIVITY

The potential production rates which correspond to the critical maximum casting speeds presented in the previous section are shown in Figures 15 and 16. Figure 16 shows that the natural increase in productivity with increasing section size outweighs the decrease in casting speed needed to achieve the larger critical shell thickness necessary for larger section sizes. Thus, the maximum productivity can be obtained with the largest section sizes.

The theoretical maximum casting speeds and productivities predicted in this work are huge and are much larger than experienced in current practice. Thus, it would appear that the shell easily has the strength necessary to contain the liquid pool at mold exit for most cases. The true obstacles which limit productivity are the inability to satisfy the other criteria discussed in the introduction. Specifically, the lack of a uniform shell thickness and the lack of continuous liquid flux lubrication are likely the limiting criteria in practice.

Attention should return to other problems which limit casting productivity. To improve the likelyhood of achieving uniform shell growth and a continuous liquid flux layer, it might be helpful to have less contact length with the mold. Even if mold length is decreased to only 300 mm, the theoretical casting speed of at least 15 m/min predicted in Figure 14(b) is far greater than currently can be achieved in practice. Thus, this work suggests that even shorter mold lengths should be investigated as a possible method to avoid these other problems and thereby to increase casting productivity.

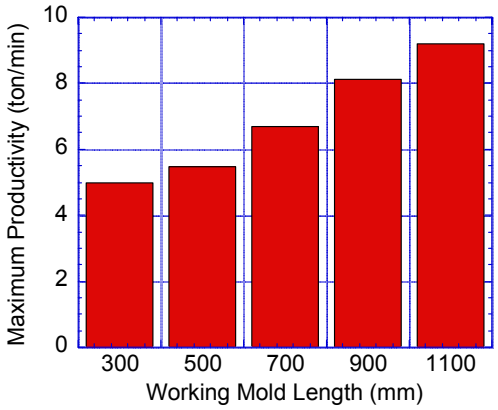

Figure 15 – Productivity increases with longer working mold length

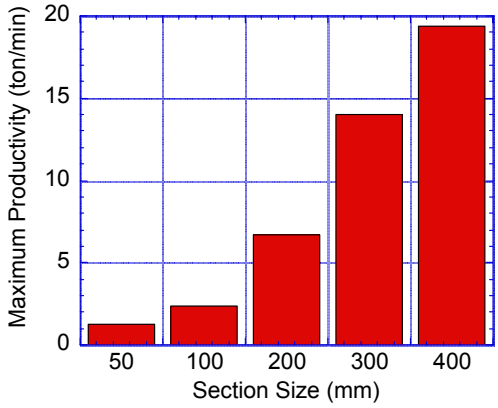

Figure 16 – Productivity increases with section size

CONCLUSIONS

This work has investigated the theoretical limits of the shell thickness, casting speed, and productivity of the steel continuous casting process as a function of steel grade, section size, and mold length, assuming ideal liquid flux lubrication. The predictions are based on the maximum casting speed that is just able to produce a thin shell with the critical thickness needed to withstand the ferrostatic pressure below the mold and avoid a longitudinal rupture from excessive creep stain. The calculations are performed with a finite-element thermal-stress model that has been validated with numerical solutions and plant data.

The critical shell thickness is predicted to be on the order of 3 mm. It is surprizingly insensitive to steel grade and superheat, but decreases with decreasing section size and increasing working mold length. The theoretical maximum casting speed and potential productivity both increase with decreasing critical shell thickness.

The theoretical limits to casting speed are predicted to be extremely high, exceeding 21 m/min for a conventional 700-mm working mold length, 200-mm square bloom mold, which corresponds to 3.5 million tonnes / year. The infeasibility of these limits in practice is likely due to other problems such as achieving shell thickness uniformity and liquid flux lubrication. Attention should return to focussing on these other problems which limit productivity. This work suggests that if shortening mold length can solve lubrication, taper, and other problems, then it should be explored as a potential means to increase productivity. A uniform shell would be strong enough to withstand the ferrostatic pressure even with a shorter mold length and a higher casting speed. To overcome the other problems which limit casting speed and productivity, design changes regarding fluid flow, mold powder, mold taper, and machine length are also required. This should be the concern of the designers of future continuous casting processes.

ACKNOWLEDGEMENTS

This work was supported by the Continuous Casting Consortium at UIUC, (AK Steel, Allegheny Ludlum, Columbus Stainless, Ispat-Inland Steel, LTV, and Stollberg, Inc.) and the National Science Foundation (Grant DMI-98-00274). The authors also wish to thank the National Center for Supercomputing Applications at UIUC for computing time for this project. Finally, the inspiration and support of the late Keith Brimacombe for the career of BGT is deeply appreciated.

REFERENCES

1. J. Lait, J.K. Brimacombe and F. Weinberg, "Mathematical Modelling of Heat Flow in the Continuous Casting of Steel," Ironmaking and Steelmaking, Vol. 2, 1974, 90-98.
2. J. Birat, M. Larrecq, J. Lamant, J. Petegnief, "The Continuous Casting Mold: A Basic Tool for Surface Quality and Strand Produtivity," Mold Operation for Quality

and Productivity, A.W. Cramb and E. Szekeres, eds., Warrendale, PA, Iron and Steel Society, 1991, 3-14.
3. K. Schwerdtfeger, "Benefits, Challenge and Limits in New Routes for Hot Strip Production," ISIJ International, Vol. 38, 8, 1998, 852-861.
4. J.-K. Park, I.V. Samarasekera, B.G. Thomas, U.-S. Yoon, "Analysis of Thermal and Mechanical Behavior of Copper Mould During Thin Slab Casting," Steelmaking Conference Proceedings, Vol. 83, ISS, Warrendale, PA, 2000, 9-21.
5. S.N. Singh and K.E. Blazek, "Heat Transfer and Skin Formation in a Continuous Casting Mold as a Function of Steel Carbon Content," Journal of Metals, Vol. 26, 1974, 17-27.
6. A. Grill, K. Sorimachi and J.K. Brimacombe, "Heat Flow, Gap Formation and Break-Outs in the Continuous Casting of Steel Slabs," Metallurgical Transactions, Vol. 7B, 1976, 177-189.
7. I.V. Samarasekera and J.K. Brimacombe, "The Thermal Field in Continuous-Casting Moulds," Canadian Metallurgical Quarterly, Vol. 18, 1979, 251-266.
8. A. Grill, J.K. Brimacombe and F. Weinberg, "Mathematical analysis of stresses in continuous casting of steel," Ironmaking and Steelmaking, Vol. 3, 1, 1976, 38-47.
9. K. Sorimachi and J.K. Brimacombe, "Improvements in mathematical modelling of stresses in continuous casting of steel," Ironmaking and Steelmaking 4, 1977, 240-245.
10. J.K. Brimacombe, F. Weinberg and E.B. Hawbolt, "Formation of Longitudinal, Midface Cracks in Continuously-Cast Slabs," Metallurgical Transactions B, Vol. 10B, 1979, 279-292.
11. R.B. Mahapatra, J.K. Brimacombe and I.V. Samarasekera, "Mold Behavior and Its Influence on Quality in the Continuous Casting of Steel Slabs: Part II. Mold Heat Transfer, Mold Flux Behavior, Formation of Oscillation Marks, Longitudinal Off-Corner Depressions, and Subsurface Cracks," Metallurgical Transactions B, Vol. 22B, 1991, 875-888.
12. J.K. Brimacombe, "Design of Continuous Casting Machines Based on a Heat-Flow Analysis: State-of-the-Art Review," Canadian Metallurgical Quarterly, Vol. 15, 2, 1976, 163-175.
13. J.K. Brimacombe, P.K. Agarwal, S. Hibbins, B. Prabhaker, L.A. Baptista, "Spray Cooling in Continuous Casting," Continuous Casting, Vol. 2, J.K. Brimacombe, eds., ISS, Warrendale, PA, 1984, 105-123.
14. J. Knowepke, M. Hubbard, J. Kelly, R. Kittridge, J. Lucas, "Pencil Blister Reduction at Inland Steel Company," Steelmaking Conference Proceedings, Vol. 77, ISS, Warrendale, PA, 1994, 381-388.
15. B.G. Thomas, A. Dennisov and H. Bai, "Behavior of Argon Bubbles during Continuous Casting of Steel," Steelmaking Conference Proceedings, Vol. 80, Chicago, IL, ISS, Warrendale, PA., 1997, 375-384.
16. H. Zhu, "Coupled Thermal-Mechanical Fixed-Grid Finite-Element Model with Application to Initial Solidification," PhD Thesis, University of Illinois, 1997.
17. B.G. Thomas and J.T. Parkman, "Simulation of Thermal Mechanical Behavior during Initial Solidification," Thermec 97 Internat. Conf. on Thermomechanical

Processing of Steel and Other Materials, Vol. 2, T. Chandra, eds., Wollongong, Australia, TMS, 1997, 2279-2285.
18. Y.-M. Won, "Effect of Cooling Rate on ZST, LIT, ZDT of Carbon Steels Near Melting Point," ISIJ International, Vol. 38, 10, 1998, 1093-1099.
19. Y.-M. Won, T.J. Yeo, D.J. Seol, K.H. Oh, "A New Criterion for Crack Formation in Continuous Casting Steels," in press, 2000,
20. K. Harste, A. Jablonka and K. Schwerdtfeger, "Shrinkage and Formation of Mechanical Stresses during Solidification of Round Steel Strands," Paper presented at 4th Int. Conf. on Continuous Casting, Centres de Recherches Metallurgiques and Verein Deutscher Eisenhuttenleute, 1988, Stahl und Eisen, Brussels, 633-644.
21. I. Jimbo and A. Cramb, "The density of liquid iron-carbon alloys," Metallurgical Transactions B, Vol. 24B, 1993, 5-10.
22. P.J. Wray, "Plastic Deformation of Delta-Ferritic Iron at Intermediate Strain Rates," Metall. Trans. A, Vol. 7A, Nov., 1976, 1621-1627.
23. P. Kozlowski, B.G. Thomas, J. Azzi, H. Wang, "Simple Constitutive Equations for Steel at High Temperature," Metallurgical Transactions A, Vol. 23A, March, 1992, 903-918.
24. J.H. Weiner and B.A. Boley, "Elasto-plastic thermal stresses in a solidifying body," J. Mech. Phys. Solids, Vol. 11, 1963, 145-154.